LETTER

Hidden-symmetry–protected topological phases on a one-dimensional lattice

To cite this article: Linhu Li and Shu Chen 2015 *EPL* **109** 40006

A Letters Journal Exploring the Frontiers of Physics

February 2015

EPL, **109** (2015) 40006 www.epljournal.org
doi: 10.1209/0295-5075/109/40006

Hidden-symmetry–protected topological phases on a one-dimensional lattice

Linhu Li[1] and Shu Chen[1,2]

[1] *Beijing National Laboratory for Condensed Matter Physics, Institute of Physics, Chinese Academy of Sciences Beijing 100190, China*
[2] *Collaborative Innovation Center of Quantum Matter - Beijing, China*

received 7 November 2014; accepted in final form 5 February 2015
published online 25 February 2015

PACS 03.65.Vf – Phases: geometric; dynamic or topological
PACS 71.10.Fd – Lattice fermion models (Hubbard model, etc.)

Abstract – We demonstrate the existence of a topologically nontrivial phase in a one-dimensional fermionic lattice system subjected to synthetic gauge fields, which is beyond the standard Altland-Zirnbauer classification of topological insulators. The topological phase can be characterized by the presence of degenerate zero-mode edge states or a quantized Berry phase of the occupied Bloch band. By analyzing symmetries of the system, we identify that the topological phase and zero-mode edge states are protected by two hidden symmetries. An extended model with hidden symmetry breaking is also studied in order to reveal the effect of hidden symmetries on the symmetry-protected topological phase.

Introduction. – Exploring nontrivial topological states has attracted wide interest in various fields of physics as stimulated by the rapid progress in the study of topological insulators [1]. Due to their relatively simple geometrical structures and good tunability, one-dimensional (1D) systems with topologically nontrivial phases have attracted intense recent studies [2–20] with a series of experimental progress which has been made in hybrid superconductor-semiconductor wires [2,3], photonic crystals [4], cold atomic gases [5] and microwave settings [6]. Depending on its global discrete symmetries, such as time-reversal symmetry, particle-hole symmetry and chiral symmetry, a 1D fermion system can be classified into ten different symmetry classes [21], and five of them support topological states [22–24]. Typical 1D topological models, such as the SSH model (class BDI) [7] and Kitaev's Majorana chain model (class D) [8], belong to the standard tenfold symmetry class [22,23]. A model of symmetry class AIII has been proposed for cold fermions subjected to artificial gauge fields on a 1D optical lattice [9]. 1D topological models in class DIII [16–18] and class CII [18] have also been studied very recently.

While there exist only five topologically nontrivial classes in the standard Altland-Zirnbauer classification [21–24], topological classification has been enriched when some other symmetries, *e.g.*, the reflection symmetry [25] and the inversion symmetry [26,27], are considered in addition to the time-reversal, particle-hole and chiral symmetries. In principle, for every discrete symmetry, there exist corresponding topological insulating phases with distinct physical properties related to the specific symmetry. Usually, these topologically nontrivial states protected by specific symmetries belong to the category of the symmetry-protected topological (SPT) state, which can be defined as a state with trivial bulk spectrum, but nontrivial boundary spectrum when and only when the system including the boundary preserves the same specific symmetries [28–30].

As most of the studied models [7–18] can be classified into tenfold Altland-Zirnbauer classes, it is interesting to search for topologically nontrivial models beyond the standard classification. In this work, we present a 1D topological model, which cannot be classified into the standard ten-fold classes but is protected by some unusual hidden symmetries. By tuning parameters of the model, the system can be a conductor, a trivial insulator or a topological insulator characterized by the quantized Berry phase [31–33]. The topologically nontrivial phase supports doubly degenerate zero-mode edge states, which are protected by both a hidden chiral symmetry and a hidden combination symmetry of the inversion and complex conjugation. By adding an additional spin-flip term,

which breaks the hidden chiral symmetry, the zero-mode edge states no longer exist, but the model can still support topologically nontrivial phase with degenerate edge states protected by the hidden combination symmetry. In this case, the model can be viewed as an extended version of the Creutz ladder model, as it can be mapped to the Creutz ladder model [34] at some special parameter regimes.

Model. – We consider a tight-binding model of two-component fermionic atoms loaded in a 1D lattice. The atoms are subjected to a synthetic gauge potential and a Zeeman field M_z, which can be described by the tight-binding Hamiltonian

$$H_1 = \sum_{n,ss'} \hat{c}^\dagger_{n,s} U_{ss'} \hat{c}_{n+1,s'} + \text{h.c.} + M_z(\hat{c}^\dagger_{n,\uparrow}\hat{c}_{n,\uparrow} - \hat{c}^\dagger_{n,\downarrow}\hat{c}_{n,\downarrow}), \quad (1)$$

where s labels the two components (up and down arrows) of the fermions and the tunneling matrix can be written as

$$U = \begin{pmatrix} -te^{i\theta} & t_s \\ t_s & -te^{-i\theta} \end{pmatrix}. \quad (2)$$

For convenience, we set $t = 1$ as the energy unit in the following context. This model may be realized in two-component fermion systems with artificial gauge potentials.

For the system under the period boundary condition (PBC), its energy spectrum is easily calculated through a Fourier transformation $\hat{c}_{n,s} = 1/\sqrt{L}\sum_k e^{ikn}\hat{c}_{k,s}$ with L the number of lattice sites. In the momentum space, the Hamiltonian can be written as

$$H_1 = \sum_k \hat{\psi}^\dagger_k h(k) \hat{\psi}_k, \quad (3)$$

where $\hat{\psi}^\dagger_k = (\hat{c}^\dagger_{k,\uparrow}, \hat{c}^\dagger_{k,\downarrow})$ and $h(k) = d_0(k)I + d(k)\cdot\sigma$ with I the identity matrix, and $\sigma = (\sigma_x, \sigma_y, \sigma_z)$ the Pauli matrices acting on the spin vector $\hat{\psi}_k$, $d_0(k) = -2\cos\theta\cos k$, $d_x(k) = 2t_s\cos k$, $d_y(k) = 0$, $d_z(k) = 2\sin\theta\sin k + M_z$. The eigenenergies are

$$E_\pm(k) = d_0(k) \pm \sqrt{d_x^2(k) + d_z^2(k)}. \quad (4)$$

In the absence of t_s, the two components of fermions are independent of each other. A nonzero θ shifts the two bands to the left and the right, respectively, in the Brillouin zone, and M_z moves the two bands up and down, as shown in fig. 1(a) and (b). Further increasing the value of M_z will separate the two bands completely by opening a gap between them, and the system becomes a trivial insulator. Adding a spin-flip term of t_s will mix bands of different components of fermions. As shown in fig. 1(c), a term of $t_s = 0.1$ lifts the degeneracy of crossing points of bands in fig. 1(b). When $t_s = 1$, the up and down bands are completely separated by a gap at $k = -\pi/2$ (fig. 1(d)). In fig. 1(d)–(f), we display the spectrum with

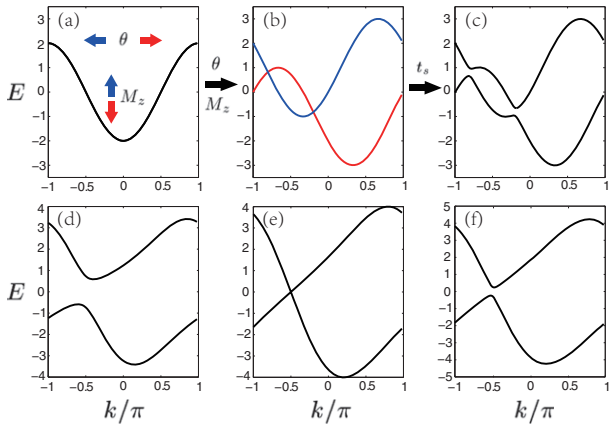

Fig. 1: (Color online) The spectrum in the momentum space. (a) $M_z = t_s = \theta = 0$; (b) $M_z = 1$, $\theta = \pi/3$, $t_s = 0$; (c) $M_z = 1$, $\theta = \pi/3$, $t_s = 0.1$; (d)–(f) $\theta = \pi/3$, $t_s = 1$, $M_z = 1$, $\sqrt{3}$, and 2, respectively. Panels (a)–(c) show the different effect of each parameter, and panels (d)–(f) show the variance of spectrum *vs.* M_z, which indicates the existence of a phase transition induced by varying M_z.

$\theta = \pi/3$, $t_s = 1$ and different M_z. It is shown that the gap is closed at $M_z = \sqrt{3}$ and reopened with further increasing M_z, which indicates that a quantum phase transition can be induced by varying M_z with the transition point determined by the gap closing point.

Edge states. – Next we unveil that the phase transition induced by M_z is a topological phase transition. For 1D systems, a hallmark of the topological phase is the emergence of degenerate edge states under the open boundary condition (OBC). To determine whether the phase transition is topological or not, we diagonalize the Hamiltonian under the OBC, and illustrate its energy spectrum. Defining the single particle state as $\Psi = \sum_n^L(\phi_{n,\uparrow}\hat{c}^\dagger_{n,\uparrow} + \phi_{n,\downarrow}\hat{c}^\dagger_{n,\downarrow})|0\rangle$, from $H\Psi = E\Psi$, we have the eigenequations:

$$\begin{aligned} E\phi_{n,\uparrow} =& -[e^{i\theta}\phi_{n+1,\uparrow} + e^{-i\theta}\phi_{n-1,\uparrow}] \\ &+ t_s[\phi_{n+1,\downarrow} + \phi_{n-1,\downarrow}] + M_z\phi_{n,\uparrow}, \\ E\phi_{n,\downarrow} =& -[e^{-i\theta}\phi_{n+1,\downarrow} + e^{i\theta}\phi_{n-1,\downarrow}] \\ &+ t_s[\phi_{n+1,\uparrow} + \phi_{n-1,\uparrow}] - M_z\phi_{n,\downarrow}. \end{aligned} \quad (5)$$

Numerically solving eqs. (5) under the OBC of $\phi_{0,s} = \phi_{L+1,s} = 0$, we can obtain the energy spectrum of the system. In fig. 2(a), we display the energy spectra for the open chain with $\theta = \pi/3$, $t_s = 1$ and $L = 100$ as a function of M_z. It is clear that the gap closed at $M_{zc} \approx 1.73$ and reopened when $M_z > M_{zc}$, which is consistent with the spectra under PBC as shown in fig. 1(d)–(f). The novel phenomena here is the emergence of zero-mode states for the system under OBC in the regime of $M_z < M_{zc}$. As shown in fig. 2(b), (c), the particle density distributions $\rho_n = |\phi_{n,\uparrow}|^2 + |\phi_{n,\downarrow}|^2$ of the doubly degenerate zero-mode states indicate that they are edge states localized at the opposite ends of the chain. The existence or absence of

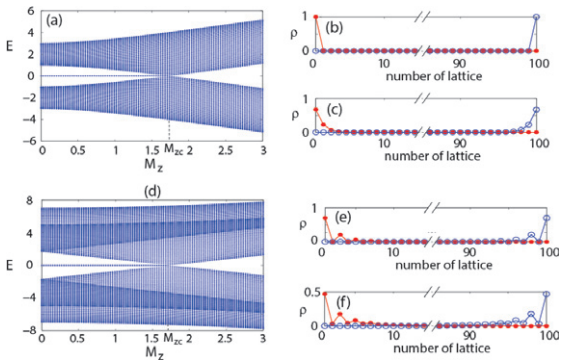

Fig. 2: (Color online) Panels (a) and (d) show spectra of two different systems under the OBC *vs.* M_z, and figures on the right show density distributions ρ of zero modes for corresponding systems on the left of figures. The parameters are: (a)–(c) $t_s = 1$ and $\theta = \pi/3$. Particularly, we have $M_z = 0$ for (b) and $M_z = 1$ for (c); (d)–(f) $t_s = 3$ and $\theta = \pi/3$. For (e) and (f), we have $M_z = 0$ and $M_z = 1$, respectively. The phase transition points in (a) and (d) are both $M_{zc} \approx 1.73$.

zero modes in the regime of $M_z < M_{zc}$ or $M_z > M_{zc}$ suggests that the phase transition occurring at M_{zc} is topologically nontrivial.

Next we show that these edge states can be achieved analytically in some special parameter regions. To see it clearly, first we reorganize the wave amplitudes $\phi_{n,s}$ as

$$f_n = \phi_{n,\downarrow} - e^{i\beta}\phi_{n,\uparrow}, \quad g_n = \phi_{n,\uparrow} - e^{i\beta}\phi_{n,\downarrow}, \tag{6}$$

with $e^{i\beta} = \frac{\cos\theta}{t_s} + i\sqrt{1 - \frac{\cos^2\theta}{t_s^2}}$. With these new defined functions, requiring the eigenenergy $E = 0$, eqs. (5) can be decoupled as

$$\begin{aligned} -M_z f_n + i\mu_+ f_{n+1} + i\mu_- f_{n-1} &= 0, \\ M_z g_n + i\mu_- g_{n+1} + i\mu_+ g_{n-1} &= 0 \end{aligned} \tag{7}$$

with $\mu_+ = \sqrt{t_s^2 - \cos^2\theta} + \sin\theta$, $\mu_- = \sqrt{t_s^2 - \cos^2\theta} - \sin\theta$, and $n = 1, 2, \ldots, L$. In terms of the transfer matrix form, f_n and g_n can be written as

$$\begin{pmatrix} f_{n+1} \\ f_n \end{pmatrix} = F \begin{pmatrix} f_n \\ f_{n-1} \end{pmatrix}, \quad \begin{pmatrix} g_{n-1} \\ g_n \end{pmatrix} = G \begin{pmatrix} g_n \\ g_{n+1} \end{pmatrix}, \tag{8}$$

where

$$F = \begin{pmatrix} \frac{M_z}{i\mu_+} & -\frac{\mu_-}{\mu_+} \\ 1 & 0 \end{pmatrix}, \quad G = \begin{pmatrix} \frac{-M_z}{i\mu_+} & -\frac{\mu_-}{\mu_+} \\ 1 & 0 \end{pmatrix}. \tag{9}$$

Without loss of generality, we shall focus on the regime of $\theta \in (0, \pi)$ with $\sin\theta > 0$ in the following calculation.

For $t_s = \pm 1$ and general M_z, the corresponding equations give solutions of $f_n = (\frac{M_z}{2i\sin\theta})^{n-1}$ and $g_n = (\frac{M_z}{2i\sin\theta})^{L-n}$ when $|M_z| < 2\sin\theta$ and $L \gg 1$, which decrease exponentially from one end to another. For the case with $M_z = 0$ and general t_s, the solutions have the forms of $f_{2m-1} = (-\frac{\mu_-}{\mu_+})^{m-1}$ and $g_{2m} = (-\frac{\mu_-}{\mu_+})^{\frac{L}{2}-m}$, with $f_{2m} = g_{2m-1} = 0$ and $m = 1, 2, \ldots, L/2$ for even number of lattice sites L. For odd L, these two zero-mode solutions have expressions similar to the ones of the even case, but both f_n and g_n have nonzero values only when $n = 2m - 1$, with $m = 1, 2, \ldots, (L+1)/2$. These edge modes also decay exponentially, and exist only when $L \gg 1$ and $|t_s| > |\cos\theta|$. The density distributions of zero-mode states of these two cases are given in fig. 2(c) and (e), respectively.

For a general case with $M_z \neq 0$ and $t_s \neq \pm 1$, the edge modes can be obtained by numerically solving eqs. (7) as shown in fig. 2(f) for the example system with $t_s = 3$, $M_z = 1$ and $\theta = \pi/3$. Although the analytical solution for a general case is not accessible, we can determine the condition for the appearance of edge states by analyzing the eigenvalues of the transfer matrices in the scheme of the transfer matrix method, which has been widely used in 1D systems [35]. Assuming $F(a_f, b_f)^T = \epsilon_f(a_f, b_f)^T$, the vector $(f_1, f_0)^T = (f_1, 0)^T$ can be always written as a linear superposition of the two eigenvectors of F, *i.e.*, $(f_1, 0)^T = s_1(a_{f,1}, b_{f,1})^T + s_2(a_{f,2}, b_{f,2})^T$, with s_1 and s_2 the superposition coefficients. Thus from eq. (8) we have $(f_{n+1}, f_n)^T = F^n(f_1, f_0)^T$, *i.e.*,

$$\begin{pmatrix} f_{n+1} \\ f_n \end{pmatrix} = s_1\epsilon_{f,1}^n \begin{pmatrix} a_{f,1} \\ b_{f,1} \end{pmatrix} + s_2\epsilon_{f,2}^n \begin{pmatrix} a_{f,2} \\ b_{f,2} \end{pmatrix}, \tag{10}$$

which suggests that $f_n = 0$ as $n \to \infty$, *i.e.*, the eigenstate localized at the edge of f_1, if the modulus of each eigenvalue of F are smaller than unity. By solving the characteristic equation of F, we can achieve $\epsilon_{f,1} = \pm i\mu_-/\mu_+$ and $\epsilon_{f,2} = \mp i$ while $M_z = \pm 2\sin\theta$. Noticing $|\epsilon_{f,1}| < 1$ when $|t_s| > |\cos\theta|$ and $|\epsilon_{f,2}| = 1$ with this specific M_z, we can infer that $M_z = \pm 2\sin\theta$ are transition points, which separate regimes with and without edge states. With further analyzing of the characteristic equation, we find that $|\epsilon_{f,1}|$ decreases with the increase of $|M_z|$, whereas $|\epsilon_{f,2}|$ increases with the increase of $|M_z|$. Hence $|\epsilon_{f,2}|$ will exceed unity when $|M_z| > 2\sin\theta$, while the maximum of $|\epsilon_{f,1}|$ is $|\epsilon_{f,1}(M_z = 0)| = |\sqrt{\mu_-/\mu_+}| < 1$. Thus we have the conclusion that the zero-mode edge states f only exists when $|M_z| < 2\sin\theta$. A similar discussion can be applied to g_n and G as well, while it is localized at the opposite end from f_n. The above discussion shows that as long as $|t_s| > |\cos\theta|$, topological phase transition points $M_{zc} = \pm 2\sin\theta$ are irrelevant to t_s. This conclusion is also supported by the numerical results in fig. 2(a) and (d).

The condition $|M_z| < 2\sin\theta$ also indicates that no zero-mode edge states could exist if $\theta = 0$ and π. Although the above discussion is limited in the regime of $\theta \in (0, \pi)$, for the case in the regime of $\theta \in (\pi, 2\pi)$ with $\sin\theta < 0$, following similar procedures we can achieve the condition for the existence of zero-mode edge modes given by $|M_z| < -2\sin\theta$, and the two edge modes f and g localized at the other ends opposite to the ones above. These conditions suggest that the topological properties of this model are similar for θ and $-\theta$. As illustrated in fig. 3(a), the spectrum under OBC *vs.* θ is symmetric about $\theta = 0$, and

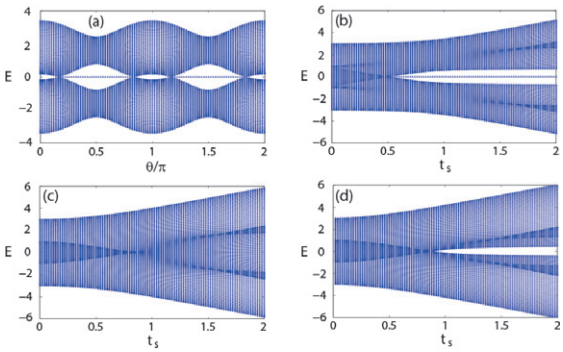

Fig. 3: (Color online) The OBC spectrum *vs.* different parameters. (a) $M_z = 1$, $t_s = 1$; (b) $M_z = 1$, $\theta = \pi/3$; (c) $M_z = 1$, $\theta = \pi/6$; (d) $M_z = 1$, $\theta = \pi/12$.

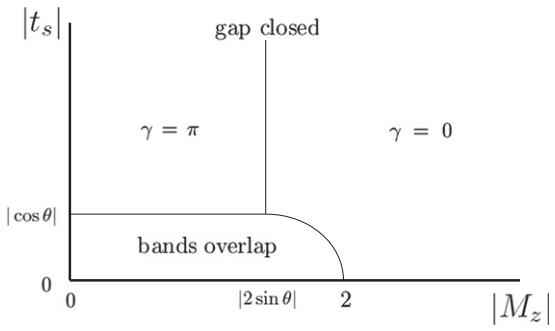

Fig. 4: The phase diagram of this model. The region with $\gamma = \pi$ indicates a topologically nontrivial insulator and the one with $\gamma = 0$ indicates a trivial insulator. The gap overlap region indicates a conductor.

varying θ while fixing other parameters will also induce a topological phase transition with the topologically nontrivial (trivial) phase characterized by the presence (absence) of degenerate zero modes. In fig. 3(b)–(d), we also display spectra of systems under the OBC *vs.* t_s by fixing $M_z = 1$ and θ, with $\theta = \pi/3$, $\pi/6$ and $\pi/12$, respectively. While there always exists a conductor phase for different θ in the regime of $|t_s| < |\cos\theta|$, there exist different phases in the regime of $|t_s| > |\cos\theta|$ depending on whether $\sin\theta$ is larger or smaller than 1/2. We will further discuss the phase boundary condition in the next section.

Topological invariant and phase diagram. – The existence of zero-mode edge states is attributed to the nontrivial topology of the corresponding bulk system, which can be characterized by the Berry phase of the occupied Bloch band. In the momentum space, the Berry phase is defined as

$$\gamma = \int_{-\pi}^{\pi} \mathrm{d}k \langle u_k | i\partial_k | u_k \rangle, \tag{11}$$

where u_k denotes the occupied Bloch states which are eigenstates of the Hamiltonian $h(k)$. In general, the Berry phase γ across the Brillouin zone is also referred as Zak phase [33]. For the half-filled system, the lower Bloch state is fully filled when the two bands of $h(k)$ are completely separated. The lower eigenstate of $h(k)$ is

$$|u_k\rangle = \frac{1}{\sqrt{2}} \begin{pmatrix} \mathrm{sgn}(n_x)\sqrt{1-n_z} \\ -\sqrt{1+n_z} \end{pmatrix}, \tag{12}$$

where $n_x = d_x(k)/|d(k)|$, $n_z = d_z(k)/|d(k)|$ and $|d(k)| = \sqrt{d_x^2 + d_z^2}$. By substituting (12) into (11), after some algebras one can obtain $\gamma = \frac{\pi}{2}[\mathrm{sgn}(M_z - 2\sin\theta) - \mathrm{sgn}(M_z + 2\sin\theta)]$ with a modulus 2π, which indicates $\gamma = \pi$ when $|M_z| < |2\sin\theta|$ and $\gamma = 0$ when $|M_z| > |2\sin\theta|$.

The analytical result has shown that $|M_z| = |2\sin\theta|$ separates the topologically nontrivial and trivial regimes with $\gamma = \pi$ and $\gamma = 0$. It is clear that $M_z = \pm 2\sin\theta$ are transition points, at which the energy gap is closed and the Berry phase is not well defined because of the degeneracy at the gap closing point. To establish the phase diagram, we also need to ascertain the band overlap condition, under which the system is a conductor. The two bands $E_\pm(k)$ overlap when the two branches of the eigenstates satisfied $\min[E_+(k)] < \max[E_-(k)]$. From eq. (4), we observe $E_+(k) = -E_-(\pi - k)$. Hence, the two bands will overlap if there exists a k_0 satisfied $E_+(k_0) < 0$. Basing on these conditions, we can determine phase boundaries and draw the phase diagram of the half-filled system as displayed in fig. 4.

Symmetries. – Next we analyze the symmetries of the system described by eq. (1). The system has no time-reversal symmetry, as both t_s and M_z terms break the time-reversal symmetry under the time-reversal operation $\mathcal{T} = i\sigma_y\mathcal{K}$, with $\mathcal{K}$ the complex conjugation operator. This Hamiltonian also shows no conventional chiral symmetry defined as $\mathcal{S}h(k)\mathcal{S}^{-1} = -h(k)$ in momentum space with $\mathcal{S}$ representing a specific chiral operation. However, we find that $h(k)$ satisfies

$$\sigma_x h(k) \sigma_x = -h(\pi - k), \tag{13}$$

which indicates the existence of a hidden chiral symmetry. In the case of finite number of lattice sites, we can rewrite the real space Hamiltonian into the matrix form $H = \hat{\Psi}^\dagger h \hat{\Psi}$, with $\hat{\Psi}^\dagger = (\hat{c}^\dagger_{1,\uparrow}, \hat{c}^\dagger_{2,\uparrow}, \ldots \hat{c}^\dagger_{L,\uparrow}, \hat{c}^\dagger_{1,\downarrow}, \hat{c}^\dagger_{2,\downarrow}, \ldots \hat{c}^\dagger_{L,\downarrow})$. We find that the hidden chiral operation can be realized by the operator

$$\mathcal{S} = \begin{pmatrix} 0 & \Upsilon \\ \Upsilon & 0 \end{pmatrix}, \tag{14}$$

where Υ is a $L \times L$ matrix with $\Upsilon_{n,L-n+1} = (-1)^n i$ and other elements are 0. This symmetry operator fulfills $\mathcal{S}^2 = 1$ for even L and $\mathcal{S}^2 = -1$ for odd L. Now it is straightforward to verify that the Hamiltonian satisfies the chiral symmetry [36]

$$\mathcal{S}h\mathcal{S}^{-1} = -h. \tag{15}$$

Due to the existence of the chiral symmetry, for an eigenstate $H\Phi = E\Phi$, there always exists another eigenstate $\Phi' = \mathcal{S}\Phi$, which satisfies $H\Phi' = -E\Phi'$.

Besides the hidden chiral symmetry, we find that there also exists a hidden symmetry under the operation defined as $\mathcal{V}$: $\hat{c}_{n,\uparrow} \to \hat{c}_{L-n,\uparrow}$, $\hat{c}_{n,\downarrow} \to \hat{c}_{L-n,\downarrow}$, $i \to -i$. Such an operation is a combination of the inversion and complex conjugation operations and can be written explicitly as

$$\mathcal{V} = \mathcal{K} \begin{pmatrix} \Gamma & 0 \\ 0 & \Gamma \end{pmatrix}, \tag{16}$$

where Γ is a $L \times L$ matrix with all the elements on the anti-diagonal being 1 and the other elements being 0. This operator also has the property that $\mathcal{V}^2 = 1$, and we have

$$\mathcal{V} h \mathcal{V}^{-1} = h. \tag{17}$$

The degenerate zero-mode edge states are protected by both the hidden chiral symmetry and the hidden symmetry $\mathcal{V}$. The hidden symmetry $\mathcal{V}$ indicates that if there is an edge state Φ_L with eigenenergy E_L localized at the left end, there must be another edge state $\Phi_R = \mathcal{V}\Phi_L$ with $E_R = E_L$ localized at the right end. Meanwhile, the hidden chiral symmetry indicates spectrum symmetric about $E = 0$ and leads to $E_R = -E_L$. Hence, the degenerated zero modes are protected by these symmetries together. We note that a similar situation occurs in the SSH model, for which the existence of zero modes is protected by both the chiral symmetry and inversion symmetry [37].

Extended model with symmetry breaking. – In this section, we study an extended model by adding an on-site spin-flip term on the Hamiltonian (1), which breaks the symmetries mentioned in the previous section. When either the hidden chiral symmetry or the hidden symmetry $\mathcal{V}$ is broken, zero-mode edge states are not expected to appear. Nevertheless, we find that a topologically nontrivial phase can still exist even if the hidden chiral symmetry is broken. Such a topological phase is protected by the hidden symmetry $\mathcal{V}$ and can be still characterized by the Zak phase with $\gamma = \pi$.

The Hamiltonian with the additional spin-flip term reads

$$H = H_1 + M \sum_{n=1}^{L} \hat{c}^{\dagger}_{n,\uparrow} \hat{c}_{n,\downarrow} + \text{h.c.} \tag{18}$$

In the limit case with $M_z = 0$, the extended model can be mapped to the Creutz ladder model [34] if we regard the two components of fermions as two legs of the Creutz ladder. We note that a scheme for the realization of the Creutz model in cold-atom systems has been recently proposed [38]. In the momentum space, the Hamiltonian $h(k)$ is given by $h(k) = d_0(k)I + d(k) \cdot \sigma$ with $d_0(k) = -2\cos\theta\cos k$, $d_x(k) = 2t_s \cos k + \text{Re}(M)$, $d_y(k) = -\text{Im}(M)$, $d_z(k) = 2\sin\theta\sin k + M_z$.

For a real M, the on-site spin-flip term breaks the hidden chiral symmetry. Consequently, for the system under the OBC, zero-mode edge states no longer exist due to the breaking of chiral symmetry. Nevertheless, the introduction of a real spin-flip term does not break the hidden symmetry $\mathcal{V}$ of the system,and thus a pair of degenerate edge states are still available. To see it clearly, we display the energy spectra *vs.* M in fig. 5(a) for a system with $M_z = 1$, $t_s = 1$ and $\theta = \pi/3$ under the OBC. As shown in the figure, the doubly degenerate zero-mode solutions at $M = 0$ are not stable as the eigenenergy deviates from $E = 0$ in the presence of a nonzero M term. However, a pair of degenerate midgap states still exist in a wide parameter regime with $M < M_c$, where M_c is a transition point with the gap closed. These midgap states are doubly degenerate edge states and are protected by the hidden symmetry $\mathcal{V}$. When $M > M_c$, a gap is reopened but no edge modes appear in the regime of $M > M_c$. These results indicate that the transition induced by changing M is a topological transition. Similar to the model discussed in the above sections, we can still characterize this topological phase transition by the change of the Berry phase. Following similar procedures in section II.C, we get the expression of the Berry phase of the occupied Bloch band given by $\gamma = \frac{\pi}{2}\left[\text{sgn}\left(M_z - D\right) - \text{sgn}\left(M_z + D\right)\right]$ for $M < 2t_s$ where $D = 2\sin\theta\frac{\sqrt{4t_s^2 - M^2}}{2t_s}$. The result shows that $\gamma = \pi$ in the regime of $(\frac{M}{t_s})^2 + (\frac{M_z}{\sin\theta})^2 < 4$, which agrees to the numerical results in fig. 5(b).

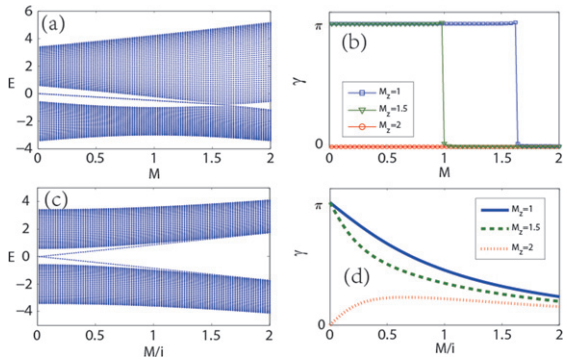

Fig. 5: (Color online) The energy spectrums and the Berry phase for the extended model. Panels (a) and (c) show the energy spectrum *vs.* the real and imaginary M, respectively, for the system with $M_z = 1$, $t_s = 1$ and $\theta = \pi/3$ under the OBC; panels (b) and (d) show the change of Berry phase as a function of real and imaginary M, respectively, for the occupied Bloch band of systems with $t_s = 1$, $\theta = \pi/3$ and different M_z. Panels (a) and (b) show the real M; panels (c) and (d) show the imaginary M.

For the case with an imaginary M, the hidden chiral symmetry is preserved, but the hidden symmetry $\mathcal{V}$ is broken. Figure 5(c) and (d) shows the energy spectrum and the Berry phase as a function of imaginary M. As the Berry phase is no longer a quantized number and the degenerate zero modes split into two branches, it clearly shows that topologically nontrivial states studied in this work are SPT states protected by the hidden symmetry $\mathcal{V}$.

Summary. – In summary, we have studied a topologically nontrivial fermion model on a 1D lattice and demonstrated the existence of a conductor phase, a trivial insulator phase and a topologically nontrivial insulator

phase for the half-filled system in different parameter regions. To unveil the nontrivial properties of the topological phase, we studied both edge states of an open chain system and the Berry phase of the corresponding bulk system in details, and identified that topological phase can be characterized by either the existence of doubly degenerate zero-mode edge states for the open system or a quantized Berry phase for the bulk system. Together with the condition of the band overlap, the phase diagram of the half-filled system is also obtained. We also analyzed the symmetry of our model and found that the topologically nontrivial phase is protected by both a hidden chiral symmetry and a hidden symmetry described by the combination of the inversion and complex conjugation operations. Finally, we examined the hidden-symmetry–protected topological phase by studying an extended model with symmetry breaking, and found that a topologically nontrivial phase can still exist if only the hidden chiral symmetry is broken. Such a topological phase can be characterized by a quantized Berry phase or the existence of a pair of degenerate non-zero-mode edge states, which is protected by the hidden combination symmetry.

* * *

This work has been supported by NSF of China under Grants No. 11374354, No. 11174360, and No. 11121063.

REFERENCES

[1] Hasan M. Z. and Kane C. L., *Rev. Mod. Phys.*, **82** (2010) 3045; Qi X.-L. and Zhang S.-C., *Rev. Mod. Phys.*, **83** (2011) 1057.

[2] Mourik V., Zuo K., Frolov S. M., Plissard S. R., Bakkers E. P. A. M. and Kouwenhoven L. P., *Science*, **336** (2012) 1003.

[3] Das A., Ronen Y., Most Y., Oreg Y., Heiblum M. and Shtrikman H., *Nat. Phys.*, **8** (2012) 887; Deng M. T., Yu C. L., Huang G. Y., Larsson M., Caroff P. and Xu H. Q., *Nano Lett.*, **12** (2012) 6414.

[4] Kraus Y. E., Lahini Y., Ringel Z., Verbin M. and Zilberberg O., *Phys. Rev. Lett.*, **109** (2012) 106402.

[5] Atala M., Aidelsburger M., Barreiro J. T., Abanin D., Kitagawa T., Demler E. and Bloch I., *Nat. Phys.*, **9** (2013) 795.

[6] Poli C., Bellec M., Kuhl U., Mortessagne F. and Schomerus H., arXiv:1407.3703.

[7] Su W. P., Schrieffer J. R. and Heeger A. J., *Phys. Rev. Lett.*, **42** (1979) 1698.

[8] Kitaev A. Y., *Phys. Usp.*, **44** (2001) 131.

[9] Liu X.-J., Liu Z.-X. and Cheng M., *Phys. Rev. Lett.*, **110** (2013) 076401.

[10] Li X., Zhao E. and Liu W. V., *Nat. Commun.*, **4** (2013) 1523.

[11] Guo H. and Shen S.-Q., *Phys. Rev. B*, **84** (2011) 195107; Guo H. and Chen S., *Phys. Rev. B*, **91** (2015) 041402.

[12] Schomerus H., *Opt. Lett.*, **38** (2013) 1912; Longhi S., *Opt. Lett.*, **38** (2013) 3716.

[13] Väyrynen J. I. and Ojanen T., *Phys. Rev. Lett.*, **107** (2011) 166804.

[14] Ganeshan S., Sun K. and Das Sarma S., *Phys. Rev. Lett.*, **110** (2013) 180403.

[15] Yan Z. and Wan S., *EPL*, **107** (2014) 47007.

[16] Wong C. L. M. and Law K. T., *Phys. Rev. B*, **86** (2012) 184516; Liu X. J., Wong C. L. M. and Law K. T., *Phys. Rev. X*, **4** (2014) 021018.

[17] Nakosai S., Budich J. C., Tanaka Y., Trauzettel B. and Nagaosa N., *Phys. Rev. Lett.*, **110** (2013) 117002; Keselman A., Fu L., Stern A. and Berg E., *Phys. Rev. Lett.*, **111** (2013) 116402.

[18] Zhao Y. X. and Wang Z. D., *Phys. Rev. B*, **90** (2014) 115158.

[19] Lang L.-J., Cai X.-M. and Chen S., *Phys. Rev. Lett.*, **108** (2012) 220401; Li L., Xu Z. and Chen S., *Phys. Rev. B*, **89** (2014) 085111.

[20] Mei F., Zhu S.-L., Zhang Z.-M., Oh C. H. and Goldman N., *Phys. Rev. A*, **85** (2012) 013638.

[21] Altland A. and Zirnbauer M. R., *Phys. Rev. B*, **55** (1997) 1142.

[22] Schnyder A. P., Ryu S., Furusaki A. and Ludwig A. W. W., *Phys. Rev. B*, **78** (2008) 195125.

[23] Ryu S., Schnyder A. P., Furusaki A. and Ludwig A. W. W., *New J. Phys.*, **12** (2010) 065010.

[24] Wen X.-G., *Phys. Rev. B*, **85** (2012) 085103.

[25] Chiu C.-K., Yao H. and Ryu S., *Phys. Rev. B*, **88** (2013) 075142.

[26] Hughes T. L., Prodan E. and Bernevig B. A., *Phys. Rev. B*, **83** (2011) 245132.

[27] Lu Y.-M. and Lee D.-H., arXiv:1403.5558.

[28] Chen X., Gu Z.-C. and Wen X.-G., *Phys. Rev. B*, **83** (2011) 035107; **84** (2011) 235128.

[29] Chen X., Gu Z.-C., Liu Z.-X. and Wen X.-G., *Science*, **338** (2012) 1604.

[30] Fidkowski L. and Kitaev A., *Phys. Rev. B*, **81** (2010) 134509; Turner A. M., Pollmann F. and Berg E., *Phys. Rev. B*, **83** (2011) 075102.

[31] Resta R., *Rev. Mod. Phys.*, **66** (1994) 899.

[32] Xiao D., Chang M.-C. and Niu Q., *Rev. Mod. Phys.*, **82** (2010) 1959.

[33] Zak J., *Phys. Rev. Lett.*, **62** (1989) 2747.

[34] Creutz M., *Phys. Rev. Lett.*, **83** (1999) 2636.

[35] Sánchez-Soto L. L., Monzón J. J., Barriuso A. G. and Cariñena J. F., *Phys. Rep.*, **513** (2012) 191.

[36] This symmetry does not hold for odd L sites with PBC. The symmetry matrix $\mathcal{S}$ works differently for odd and even lattice sites, and the hopping term for even L always connects an odd site and an even site. However, for odd L with PBC, the hopping from one end to another connects two odd sites, and breaks this symmetry. The numerical result also shows the same property.

[37] Ryu S. and Hatsugai Y., *Phys. Rev. Lett.*, **89** (2002) 077002.

[38] Mazza L., Bermudez A., Goldman N., Rizzi M., Martin-Delgado M. A. and Lewenstein M., *New J. Phys.*, **14** (2012) 015007.